Ab initio modelling of an essential mammalian protein: Transcription Termination Factor 1 (TTF1)

Kumud Tiwari[a1], Aditi Gangopadhyay[b1], Gajender Singh[a], Samarendra Kumar Singh[a*]

[a] School of Biotechnology, Institute of Science, Banaras Hindu University, Varanasi, Uttar Pradesh 221005, India

[b] Department of Chemical Technology, University of Calcutta, Kolkata, West Bengal 700009, India

[1]These authors contributed equally

[*]Corresponding author: Samarendra Kumar Singh

Cell Cycle and Cancer Laboratory, School of Biotechnology, Institute of Science, Banaras Hindu University, Varanasi, Uttar Pradesh 221005, India.

Phone: +91-8009561887, +91-8707400665

E-mail: samarendra.singh@bhu.ac.in; biotech3@rediffmail.com

Abstract

Transcription Termination Factor 1 (TTF1) is an essential mammalian protein that regulates cellular transcription, replication fork arrest, DNA damage repair, chromatin remodelling etc. TTF1 interacts with numerous cellular proteins to regulate various cellular phenomena, and plays a crucial role in maintaining normal cellular physiology, dysregulation of which has been reported towards cancerous transformation of the cells. However, despite its key role in cellular physiology, the complete structure of human TTF1 has not been elucidated to date, either experimentally or computationally. Hence, understanding the structure of human TTF1 becomes highly important for studying its functions and interactions with other cellular factors. Therefore, the aim of this study was to construct the complete structure of human TTF1 protein, using molecular modelling approaches. Owing to the lack of suitable homologues in the PDB, the complete structure of human TTF1 was constructed using *ab initio* modelling. The structural stability was determined using molecular dynamics (MD) simulations in explicit solvent, and trajectory analyses. The representative structure of human TTF1 was obtained by trajectory clustering, and the central residues were determined by centrality analyses of the residue interaction network of TTF1. Two residue clusters, in the oligomerisation domain and C-terminal domain, were determined to be central to the structural stability of human TTF1. To the best of our knowledge, this study is the first to report the complete structure of human TTF1, and the results obtained herein will provide structural insights for future research in cancer biology and related studies.

Keywords: Transcription termination, DNA binding, *ab initio* modelling, molecular dynamics simulation, network analysis, residue interaction network

Author Summary

The transcription termination factor 1 (TTF1) is an essential multifunctional mammalian protein which plays important role in regulating important cellular process like transcription, replication, DNA damage repair, chromatin remodelling etc. and its dysregulation leads to various cancers. Despite its being such an important factor, the complete structure of human TTF1 has not been determined to date, either using experimental techniques or computationally. Therefore, the aim of this study was to construct the complete structure of human TTF1 using computational modelling. In this study the complete structure of human TTF1 was constructed by *ab initio* modelling using iTasser. The stability of this model was determined by 200 ns molecular dynamics (MD) simulations. The representative conformation of human TTF1 was further determined by clustering the simulation trajectory and the residues that are central to the stability of this structure were identified. The results demonstrate the presence of two residue clusters in human TTF1, one in the oligomerisation domain and other in the C-terminal domain, which were found to be crucial for the structural stability of this protein. Hence, the results of this study will aid future studies in this field towards engineering this important protein for further biochemistry and cell biology research.

1. Introduction

Ribosomes are essential cellular organelles that partake in protein synthesis in both prokaryotes and eukaryotes. Ribosomes are comprised of ribosomal proteins and ribosomal RNA (rRNA), which is encoded by ribosomal DNA (rDNA), and serves as the catalytic subunit of the protein translation machinery. Eukaryotic rDNA is distributed in clusters of ~300-400 copies at both ends of the respective chromosomes (acrocentric chromosomes: 13,

14, 15, 21, and 22). These tandem repeats of rDNA copies create dense chromosomal regions called **N**ucleolar **O**rganizer **R**egions (**NOR**s) which consists of a non-transcribed spacer region flanked by pre-RNA coding regions. Of the total RNA that is transcribed, 80% consists of rRNAs [1,2]. Both the initiation and termination of rDNA transcription is mediated by a transcriptional regulator called Transcription Termination Factor 1 (TTF1), which is an essential protein in mammalian cells. The gene encoding TTF1 is located on **9q34.13**, in the long arm of chromosome 9. Transcription Termination Factor 1 protein (TTF1p) binds to DNA elements known as Sal box, located upstream and downstream of the rDNA gene repeats. In mammalian cells, the Sal box element consists of a *Sal*I restriction site within the 11 bp sequence, G***GGTCGACC***AG [3]. Following its discovery as a transcription regulator, subsequent studies demonstrated that TTF1 is involved in polar replication fork arrest and also acts as a chromatin remodelling factor [4,5]. Current findings demonstrate that TTF1p interacts with various DNA damage sensing proteins, including Cockayne Syndrome B (CSB) [6], Mouse Double Minute 2 (MDM2) [7] and tumor suppressor Alternative Reading Frame (ARF) [8] protein, but the mechanism and exact roles of TTF1p remains to be identified to date. The overexpression of TTF1 has been corelated in various tumours, which indicates that owing to tumor hyperproliferation, TTF1 is required in higher quantities to meet the higher rate of ribosome biogenesis in tumor cells [9–11]. The TTF1 protein has several other unidentified roles, as it appears to interact with various other factors necessary for regulating a wide variety of physiological phenomena in cells. TTF1 is truly a multifunctional protein, and hence, it becomes important to characterise the numerous unidentified roles of this protein in cellular physiology both in healthy and cancerous cells.

TTF1p has distinct functional domains, including an N-terminal regulatory domain (NRD), which also is responsible for the oligomerisation of TTF1 [12]. It has been shown that due to its oligomerisation property, TTF1p can loop the ends of rDNA together, thereby placing the promoter and terminator regions in proximity to efficiently recycle the transcription machinery, and this model is known as the "ribomotor" model [13]. Furthermore, TTF1 has a functional central domain and a C-terminal domain, which is essential for the activation and termination of Pol I-mediated transcription on a nucleosomal rDNA template [14]. The central domain has the highly conserved DNA binding myb/SANT-like domain which has strong homology with the DNA binding domain of Reb1 protein of *Schizosaccharomyces pombe,* and proto-oncoprotein c-Myb [15,16].

The only crystal structure of its yeast homolog protein, RNA Polymerase I enhancer binding protein (Reb1p) [17], bound to DNA, was solved to atomic resolution by our group [15]. The structure clearly shows an N-terminal regulatory domain which is also known as the dimerization domain, a central DNA-binding domain, and the C-terminal transcriptional terminator domain. Using various mutants, it was demonstrated that the mere binding of DNA to Reb1p is not sufficient for terminating transcription. Further it was shown that the interaction of Reb1p with Replication Protein A (RPA), via the C-terminal domain of Reb1p, is an essential requirement for effective transcriptional termination. The interaction with RPA induces an allosteric change which is necessary for stopping the movement of RNA polymerase I. Also, the domain of Reb1p which binds to DNA was identified to atomic resolution and the residues involved in protein-DNA contacts were identified. This region consists of two myb-associated domains (mybAD1 and mybAD2) and two Myb repeats

(mybR1 and mybR2). The helices involved in this region make contact with DNA at various residues [17].

TTF1 is an essential cellular protein owing to its numerous roles in several vital cellular functions, which are necessary for maintaining healthy cellular physiology. Understanding the structure of TTF1 would provide insights into the mechanistic aspect of its function. To date, there are no experimentally-determined structures or *in silico* models of TTF1. Our lab is involved in purifying and physically solving the structure of this protein. So far, crystallization trials have proved to be unsuccessful, and we are therefore attempting cryo-EM studies as well. Alternatively, computational modelling studies on this essential protein will provide a better understanding so that we can engineer the protein for future studies.

In the absence of experimentally-derived structures, homology modelling serves as a reliable method for the construction of protein structures. However, the reliability of the protein model depends on various factors, including the sequence identity between the template and target proteins. When the template-target identity falls below 30%, known as the twilight zone, the protein structure needs to be constructed by threading or *ab initio* methods [18]. This is due to the fact that below the twilight zone, the evolutionary relatedness between the template and target is doubtful, and the confidence of the prediction is low [19]. The worldwide experiment for protein structure prediction, Critical Assessment of protein Structure Prediction (CASP), ranked the iTasser (iterative threading assembly refinement) server as the best tool for *ab initio* protein modelling. In the latest CASP14 experiment conducted in 2020, the iTasser server (Zhang server) ranked the best among 47 groups

[20,21]. The iTasser server also ranked best in the previous CASP7, CASP8, CASP9, CASP10, CASP11, CASP12, and CASP13 experiments [22]. In the CASP9 experiments in 2010, the iTasser server was predicted to the best tool for protein function prediction [21]. In this study, the structure of the TTF1 protein was constructed by molecular modelling, using the iTasser server. The predicted models were validated and the structure was subjected to molecular dynamics (MD) simulations for 200 ns for studying the structural stability of TTF1, and determining the most stable conformation of the protein. Our study aimed to predict the structure of TTF1, which is an essential protein, using computational modelling. The results of our study will prove to be important for understanding the structural, functional, and therapeutic role of this essential protein.

2. Results

2.1 Sequence-based analyses

The results of sequence-based analysis with ProtParam showed that TTF1 is an unstable hydrophilic protein, as revealed by an instability index of 51.13 and grand average of hydrophobicity (GRAVY) of -0.939. This was corroborated by the results of disorder prediction, which showed that more than 50% of the residues of TTF1 are disordered (Fig 1). The results of disorder prediction further revealed that residues 1-3, 689-696, 700-701, 709, and 903-905 were disordered and had protein binding properties (S1 Fig). The physicochemical properties predicted by ProtParam and anticipation of disulphide bond (S-S) pattern by CYS REC tool are enlisted in Table 1.

Table 1: Physicochemical properties of TTF1, as determined with ProtParam.

Physicochemical Properties	**Values**
Number of residues	905
Molecular formula	$C_{4512}H_{7282}N_{1302}O_{1399}S_{28}$
Molecular weight	103 kDa
Theoretical pI	9.41
Instability index	51.13
Aliphatic index	65.09
Total number of negatively charged residues (D+E)	135
Total number of positively charged residues (R+K)	171
Extinction coefficient	96760
Grand average of hydrophobicity (GRAVY)	-0.939
Estimated half-life (mammalian reticulocyte, *in vitro*)	30 hours
S-S Bond (predicted)	22-737, 73-887, 445-892

Fig 1: Graphical representation of the disordered regions of the human TTF1 protein. Residues with disorder score ≥ 0.5 (represented by the horizontal red line) were considered to be disordered.

2.2 *Ab inito* modelling and structural validation of TTF1

The results of template search using BLASTp against the PDB revealed that the highest target-template coverage was 4%, which was well below the twilight zone for homology modelling [23]. Therefore, the structure of human TTF1 could not be modelled using the

template-based methods in comparative modelling. The complete structure of human TTF1p was therefore modelled using *ab initio* methods, using the iTasser server. The confidence of the models predicted by iTasser are indicated by the C-score, which is a confidence score that provides a measure of the quality of the models generated by iTasser. The C-scores range between -5 and 2, with higher values indicating predictions of higher confidence, while lower values of C-score indicate predictions of lower confidence [20]. In this study, the model with the highest C-score of -0.60 was selected for subsequent analyses. This model was further minimised using Yasara, and the energy minimised structure was validated using ProSA [24,25]. The results of ProSA validation revealed that the structure of TTF1 was comparable to structures of similar size in the PDB, which had been determined using X-ray crystallography (Fig 2A). Analysis of the Ramachandran plot with Procheck revealed that only 1.0% of the residues were in the disallowed regions of the plot, while 82.9% and 14.1% of the residues were in the most favoured and additional allowed regions, respectively (Fig 2B).

Fig 2: Structural validation of the energy minimised model of TTF1 using **A)** ProSA and **B)** Ramachandran plot analysis with Procheck.

2.3. Functional validation of TTF1

The results of analysis with TM-align revealed that the model of TTF1 generated by iTasser (Fig 3) was structurally most similar to cas13b (PDB ID: 6AAY), which is an RNA-binding protein from *Bergeyella zoohelcum* with RNase activity [26]. The human TTF1 protein is a DNA-binding protein that plays an important role in transcriptional termination. The TM-score of the alignment was 0.960, indicating correct topology, and the RMSD between the

generated model of TTF1 and cas13b was 2.29 Å, indicating high structural similarity between the two proteins. The structural similarity between TTF1 and cas13b indicated that the model of TTF1 obtained herein, possesses potential nucleic acid binding properties, similar to cas13b.

Fig 3: The structure of TTF1 constructed by *ab initio* modelling is depicted in light blue ribbon representation, and the structure obtained after minimisation with Yasara is depicted in dark blue ribbon representation.

The results of ligand binding analyses with COFACTOR and COACH revealed that residues 620-626 of the TTF1 model have potential binding property to the ligand phosphoaminophosphonic acid-adenylate ester (ANP). ANP is a non-hydrolysable analogue of ATP, and comprises triphosphate, adenine, and ribose sugar moieties, similar to the composition of DNA. This indicated that the model of TTF1 predicted using iTasser has potential nucleic acid binding properties, and logically relates to the DNA-binding properties of TTF1 reported in literature and also been validated in our lab using the purified TTF1 protein [3]. The ligand binding properties of the model of TTF1 were predicted to be most similar to those of the recombinase A protein of *Escherichia coli* (PDB ID: 3CMV), which possesses single-stranded DNA binding properties. These results indicated that the model of TTF1 possesses potential DNA binding properties, in agreement with the reports in existing literature and our experimental data (not shown here). The results of CD analyses revealed that residues 621-677 of TTF1 comprises the Myb-like DNA binding domain of TTF1 (pfam accession number: 13921) (S 2 Fig). The results of sequence-based CD analysis of TTF1 corroborated with the results of structure-based ligand binding site prediction by

205 COFACTOR and COACH, further validating the DNA-binding potential, and thus the
206 functional potential of the model of TTF1 constructed using iTasser. Furthermore, the
207 residues with ANP-binding properties mapped to the DNA-binding domain of TTF1,
208 implying the potential nucleotide binding properties of the structure of TTF1 generated by
209 iTasser.

210 The results of consensus-based GO prediction revealed that the molecular function of the
211 TTF1 protein model was associated with GO terms GO:0035639 (purine ribonucleoside
212 triphosphate binding), GO:0032559 (adenyl ribonucleotide binding), and GO:0043167 (ion
213 binding), with GO scores of 0.40, 0.40, and 0.39, respectively. These results further
214 confirmed the nucleotide binding properties of the structure of TTF1 obtained with iTasser.
215 The results of functional validation thus implied that the TTF1 model obtained using *ab initio*
216 modelling has potential nucleic acid-binding properties, and agrees with the data reported in
217 literature and observed in our lab.

218 **2.4. Trajectory analyses**

219 The structural model of TTF1 thus obtained by *ab initio* modelling was subjected to 200 ns
220 MD simulations for investigating the structural stability and determining any possible
221 conformational changes in TTF1. Trajectory visualisation revealed that the protein stabilised
222 after 20 ns and remained stable thereafter. This was further observed in the values of root
223 mean square deviation RMSD, which became steady after 20 ns (Fig 4). As depicted in the
224 Fig 4A, the values of RMSD became increasingly steady after 100 ns, and remained steady
225 thereafter, with fluctuations in the RMSD values being in the range of 1-1.5 Å. This indicated
226 that the system had reached equilibrium after 100 ns and remained stable thereafter. This was

further corroborated by the values of RoG (Fig 4B), which remained steady after 100 ns. The RoG is an indicator of structural compactness, and fluctuations in the values of RoG indicate protein unfolding. The fact that the values of RoG became steady after 100 ns indicated that the structure of TTF1 was stable and compact during the production run. Analysis of the values of RMSF revealed that some residues had higher flexibility, as indicated by the RMSF values, which were higher than 1.5 Å. The higher flexibility of these residues could be attributed to the fact that these residues mapped to the disordered regions predicted using DisoPred (Fig 4C).

Fig 4: Graphical representation of the values of **A)** RMSD and **B)** RoG of the protein backbone throughout the trajectory. **C)** Comparison of the average RMSF values and disorder scores of TTF1. The oligomerisation domain (residues 1-320), Myb domain 1 (residues 612-660), Myb domain 2 (residues 661-745), and chromatin remodelling region (residues 323-445) are indicated by blue, yellow, red, and green rectangles, respectively.

2.5. Representative structure of TTF1

The trajectory was clustered using Chimera v1.14, and the representative frame of the most populated cluster was selected as the representative conformation of TTF1 (Fig 5A, refer to the supplementary for coordinate file). The oligomerisation domain (residues 1-320), Myb domain 1 (residues 612-660), Myb domain 2 (residues 661-745), and chromatin remodelling region (residues 323-445,) [5,12,16] were mapped to the complete structure of TTF1 obtained herein (Fig 5B).

Fig 5: **A)** Ribbon and **B)** Surface representation of the representative structure of TTF1 obtained by trajectory clustering. The oligomerisation domain, Myb domain 1, Myb domain 2, and chromatin remodelling region are represented in blue, yellow, red, and green, respectively.

2.6. Centrality analyses

The RINs of the representative structure of TTF1 was determined using Cytoscape v3.8.2 (Fig 6), and the central residues were identified using the RINspector plugin, based on the RCA Z-scores. In the RIN, the nodes indicate the residues, while the edges represent the intra-residue interactions. Residues with RCA Z-scores ≥ 2 were considered to be central to the structural stability of the protein. As depicted in Fig 6, the residues with Z-scores ≥ 2 are coloured in yellow, and those with Z-scores ≥ 2 are represented in red. The bigger nodes indicate residues with higher values of Z-scores. The RIN revealed two interaction clusters, with one cluster being located in the oligomerisation domain of TTF1, and the other being located towards the C-terminal region of the protein (Fig 6A and 6B). The Z-scores of the residues in the interaction cluster in the oligomerisation domain were higher than those of the residues in the C-terminal domain, indicating that the interaction cluster in the oligomerisation domain plays a more crucial role in the stability of the human TTF1 protein than that of the interaction cluster in the C-terminal domain. The Z-scores of the central residues determined by centrality analysis are enlisted in Table 2.

Fig 6: The central residues of TTF1 identified by RIN and centrality analyses in the **A)** 3-dimensional structure of TTF1. **B)** The central residues in the RIN of TTF1 in 2D representation. The nodes and edges represent the residues and inter-residue interactions, respectively. The size of the nodes corresponds to the value of the RCA Z-score, with bigger nodes corresponding to residues with higher values of Z-scores. The residues with RCA Z-score ≥ 2 and ≥ 4 are indicated in yellow and red, respectively.

Table 2: Central residues of TTF1, determined by centrality analysis

Central residue	Corresponding domain	RCA Z-score	Secondary structure
K68	Oligomerisation	7.246	Loop
E196	Oligomerisation	7.2	Helix
R71	Oligomerisation	7.161	Loop
E195	Oligomerisation	7.111	Loop
Q30	Oligomerisation	7.097	Helix
HIE34	Oligomerisation	6.991	Helix
W198	Oligomerisation	6.813	Helix
R38	Oligomerisation	6.682	Helix
G202	Oligomerisation	6.555	Loop
E35	Oligomerisation	6.453	Helix
K17	Oligomerisation	6.366	Helix
E206	Oligomerisation	5.788	Helix
K31	Oligomerisation	4.573	Helix

S226	Oligomerisation	4.417	Loop
E27	Oligomerisation	4.309	Helix
T186	Oligomerisation	4.204	Loop
N228	Oligomerisation	3.947	Loop
R229	Oligomerisation	3.614	Loop
S23	Oligomerisation	3.159	Helix
I660	myb/SANT-like 1	2.83	Helix
R664	myb/SANT-like 2	2.825	Loop
K434	Chromatin remodelling	2.782	Helix
F657	myb/SANT-like 1	2.778	Helix
R164	Oligomerisation	2.769	Loop
E165	Oligomerisation	2.693	Loop
S895	-	2.693	Helix
N893	-	2.661	Loop
E882	-	2.608	Loop
T896	-	2.596	Helix
S161	Oligomerisation	2.594	Loop
Q172	Oligomerisation	2.548	Helix
E191	Oligomerisation	2.535	Loop
E431	Chromatin remodelling	2.527	Helix
G899	-	2.499	Loop
A176	Oligomerisation	2.469	Helix

S435	Chromatin remodelling	2.388	Helix
R902	-	2.326	Loop
R182	Oligomerisation	2.302	Helix
D471	-	2.069	Helix

2.7. Intra-residue hydrogen bonds

Hydrogen bonds with occupancy ≥ 75% and ≥ 85% throughout the 200 ns trajectory and in the last 50 ns, respectively, were considered to be important for the structural stability of the protein. The frequency of the hydrogen bonds throughout the trajectory and in the last 50 ns was determined using VMD. The occupancy of the intra-residue hydrogen bonds formed by the central residues is provided in S 1 Table, and the occupancy of all the intra-residue hydrogen bonds with occupancy ≥ 75% and ≥ 85% throughout the 200 ns trajectory and in the last 50 ns, respectively, are provided in the S 1 Table. The results of interaction analyses revealed that residues K17, E27, Q30, E35, R164, W198, and N228 of the oligomerisation domain, K434 of the chromatin remodelling region, and F657 of the myb/SANT-like-1 domain were most crucial to the structural stability of the protein, as indicated by the number of intra-residue hydrogen bonds and the occupancy of the hydrogen bonds throughout the trajectory.

3. Discussion

TTF1 is a crucial multifunctional nucleolar protein that regulates both transcription initiation as well as transcriptional termination of ribosomal genes by binding to specific motif

sequence and–also arrests of the replication fork in polar fashion [2]. In addition, TTF1 regulates the transcription of genes transcribed by RNA polymerase I. Using truncated human and murine TTF1 proteins, Evers and Grummt first reported species-specific sequence differences in the DNA-binding region of mammalian TTF1 [3]. Despite its major regulatory role in mammalian transcription, replication and chromatin remodelling, the complete structure of human TTF1 remains to be elucidated to date. A partial structure of human TTF1 has been predicted by AlphaFold v2.0, which uses artificial intelligence for predicting the 3-dimensional structure of proteins. However, the structure predicted by AlphaFold is partial (residues 491-866), and the remaining residues are largely unfolded, and the confidence of prediction of these unfolded regions is very low [27]. As all the residues of a protein are important for its complete regulation and function, it is necessary to consider that protein in its entirety in structural analyses. In this study, we therefore attempted to construct the complete structure of the human TTF1 protein using *ab initio* modelling and MD simulations, and also identified the residues that are central to the structural stability of human TTF1 by network analyses. To the best of our knowledge, this study is the first to report the complete structure of the human TTF1 protein (refer supplementary for coordinate file).

Owing to the lack of suitable structural homologues in the PDB with sequence coverage above the twilight zone, the structure of TTF1 was modelled using *ab initio* methods. The model of TTF1 thus obtained was subjected to functional validation and GO analysis for establishing the functional relevance. MD simulations are frequently used for obtaining atom-level insights into the structural dynamics and behaviour of biomolecular system. The stability of the model was subsequently evaluated by MD simulation for 200 ns, using an

explicit TIP4P solvent, and the trajectory was analysed for investigating structural stability and hydrogen bond frequency. The representative conformation of the human TTF1 protein was obtained by trajectory clustering, and the residues that play a central role in the structural stability of TTF1 were identified by network analysis and determination of residue centrality. The results of RIN analysis and computation of centrality measures revealed two interaction clusters in the structure of human TTF1, with one in the oligomerisation domain of TTF1 and the other in the C-terminal domain. The data further indicated that the residue cluster in the oligomerisation domain plays a more significant role in the stability of TTF1, compared to that in the C-terminal domain. The N-terminal oligomerization domain has been shown to play important regulatory function [2] while the C-terminal domain is involved in transcription termination [5]. In the absence of experimentally-derived structural data pertaining to the human TTF1 protein, we believe that the results of our study provide valuable structural information, including domain architecture, and their characteristics, among others. Hence, our study could facilitate future studies aimed towards understanding the mechanism underlying the function of the human TTF1, including its interaction with other protein, and for engineering this protein with the purpose of solving its physical structure, drug design and therapeutic applications etc.

4. Conclusion

Conclusively, this is very first study to report complete structure of the essential human TTF1 protein, using computational modelling, and identify the residues and its characteristics that are central to the structural stability of the protein.

5. Materials and Methods

5.1 Sequence retrieval and sequence-based analyses

The sequence of TTF1 was retrieved from UniProtKB (UniProtKB accession number: Q15361). The physicochemical properties of TTF1 were analyzed using ProtParam [28], and the disorder profile was analyzed using DisoPred version 3.1 [29,30].

5.2 *Ab initio* modelling of TTF1

The structural homologues of human TTF1 in the PDB was searched using BLASTp and threading-based approaches, for identifying suitable templates for homology modelling. Owing to the lack of suitable structural templates, the structure of human TTF1 was modelled using *ab initio* modelling, using the iTasser server [20]. In the iTasser algorithm, the final models are selected using the SPICKER program for clustering the generated structures. The structure of TTF1 generated by iTasser was initially minimised using the Yasara energy minimization server, with the Yasara force field [24]. The energy minimised structure was then validated using Ramachandran plot analysis and ProSA [31,32].

5.3 Functional validation of TTF1 constructed by *ab initio* modelling

The models generated by iTasser were functionally validated using the TM-align program for determining the structures in the PDB that are structurally, and thus functionally, similar to the models of TTF1p constructed by *ab initio* modelling. The TM-align program was used to identify structures in the PDB that are structurally similar to the model generated by iTasser. This program determines the similarity between proteins on the basis of the TM-score, a scoring function that provides a quantitative measure of topological similarity between proteins [33]. It provides a measure of structural similarity, with values > 0.5

indicating models of correct topology [34]. The models were further validated using the COACH and COFACTOR programs for predicting the ligand binding sites, based on the similarity of the protein folds with functional templates [35,36]. The result of ligand binding site prediction was mapped to the results of sequence-based conserved domain (CD) analyses using the CD search tool of NCBI [37]. The molecular function of the modelled protein was further validated by consensus-based gene ontology (GO) search.

5.4 MD simulations

The model of TTF1 obtained by *ab initio* modelling was subjected to MD simulations for 200 ns using Flare v4, which is based on the OpenMM Toolkit, for studying the structural stability and determining any possible conformational changes of TTF1p. The protein was then prepared in Flare v4 at pH 7.4, and solvated in TIP4P solvent using a buffer of 10 Å thickness. The system was subsequently neutralised by the addition of 28 Cl^- ions. The system was then minimized until the energy tolerance reached 0.25 Kcal/mol, and subsequently equilibrated for 200 ps. It was then finally subjected to 200 ns MD simulations at a temperature of 298 K and a pressure of 1 bar, using the XED force field and the NPT ensemble. The timestep was set to 2 fs.

The values of root mean square deviation (RMSD), root mean square fluctuations (RMSF), and radius of gyration (RoG) of the protein backbone throughout the trajectory was analyzed using the vmdICE plugin in VMD v1.9.3 [38,39]. The occupancy of the inter-residue hydrogen bonds throughout the 200 ns trajectory and in the last 50 ns was determined using VMD v1.9.3. The portion of the trajectory following equilibration was clustered using

Chimera v1.14, and the representative frame of the most populated cluster was selected as the representative conformation of TTF1p [40].

5.5 Determination of residue interaction networks (RINs) and centrality analysis

The RINs of TTF1p were determined using the RINalyzer plugin in Cytoscape v3.8.2 [41,42]. The network centrality measures were computed using the RINspector plugin in Cytoscape v3.8.2, based on the residue centrality analysis (RCA) Z-score.

Conflicts of interest

The authors have no conflicts of interest to declare.

Acknowledgement

The authors are thankful to the Director Prof. A.K. Tripathi and Coordinator Prof. S.M. Singh, School of Biotechnology, Institute of Science, Banaras Hindu University for providing space and facilities to conduct the research. We thank Dr. V.K. Singh for providing valuable suggestions during the study. We are thankful to Department of Biotechnology, Govt. of India for funding Samarendra K Singh (SKS) and Kumud Tiwari (KT) with grant and fellowship respectively. Author Aditi Gangopadhyay (AG) acknowledges the Council of Scientific and Industrial Research (CSIR), New Delhi, for providing financial assistance. We also thank CSIR for funding the fellowships of Gajender Singh (GS).

Author contribution

SKS was involved in the Conceptualization and designing; Supervision; Writing - critical review & editing of the manuscript. KT and AG involved in Data curation; Formal analyses;

Investigation; Methodology; Project administration; Resources; Software; Validation; Visualization; Writing - original draft; review & editing of the manuscript. GS contributed analyses tools and data; Visualization; Writing – original draft.

Funding statement

The research was funded by Department of Biotechnology (DBT), Govt. of India, RLS grant (BT/RLF/Re-entry/43/2016) to SKS and JRF fellowship to KT. Council of Scientific and Industrial Research (CSIR) also supported this research by funding AG (RA grant number: 09/028(1088)2019-EMR-I) and GS (JRF) by awarding fellowships.

References

1. Zhou H, Wang Y, Lv Q, Zhang J, Wang Q, Gao F, et al. Overexpression of ribosomal RNA in the development of human cervical cancer is associated with rDNA promoter hypomethylation. PLoS One. 2016;11: e0163340. doi:10.1371/journal.pone.0163340

2. Akamatsu Y, Kobayashi T. The Human RNA Polymerase I Transcription Terminator Complex Acts as a Replication Fork Barrier That Coordinates the Progress of Replication with rRNA Transcription Activity. Mol Cell Biol. 2015;35: 1871–1881. doi:10.1128/mcb.01521-14

3. Evers R, Grummt I. Molecular coevolution of mammalian ribosomal gene terminator sequences and the transcription termination factor TTF-I. Proc Natl Acad Sci U S A. 1995;92: 5827–5831. doi:10.1073/pnas.92.13.5827

4. Pütter V, Grummt F. Transcription termination factor TTF-I exhibits contrahelicase activity during DNA replication. EMBO Rep. 2002;3: 147–152. doi:10.1093/embo-reports/kvf027

5. Längst G, Blank TA, Becker PB, Grummt I. RNA polymerase I transcription on nucleosomal templates: The transcription termination factor TTF-I induces chromatin remodeling and relieves transcriptional repression. EMBO J. 1997;16: 760–768. doi:10.1093/emboj/16.4.760

6. Aamann MD, Muftuoglu M, Bohr VA, Stevnsner T. Multiple interaction partners for Cockayne syndrome proteins: Implications for genome and transcriptome maintenance. Mech Ageing Dev. 2013;134: 212–224. doi:10.1016/j.mad.2013.03.009

7. Lessard F, Stefanovsky V, Tremblay MG, Moss T. The cellular abundance of the essential transcription termination factor TTF-I regulates ribosome biogenesis and is determined by MDM2 ubiquitinylation. Nucleic Acids Res. 2012;40: 5357–5367. doi:10.1093/nar/gks198

8. Lessard F, Morin F, Ivanchuk S, Langlois F, Stefanovsky V, Rutka J, et al. The ARF Tumor Suppressor Controls Ribosome Biogenesis by Regulating the RNA Polymerase I Transcription Factor TTF-I. Mol Cell. 2010;38: 539–550. doi:10.1016/j.molcel.2010.03.015

9. Stults DM, Killen MW, Williamson EP, Hourigan JS, Vargas HD, Arnold SM, et al. Human rRNA gene clusters are recombinational hotspots in cancer. Cancer Res.

2009;69: 9096–9104. doi:10.1158/0008-5472.CAN-09-2680

10. Komatsu H, Iguchi T, Ueda M, Nambara S, Saito T, Hirata H, et al. Clinical and biological significance of transcription termination factor, RNA polymerase i in human liver hepatocellular carcinoma. Oncol Rep. 2016;35: 2073–2080. doi:10.3892/or.2016.4593

11. Ueda M, Iguchi T, Nambara S, Saito T, Komatsu H, Sakimura S, et al. Overexpression of Transcription Termination Factor 1 is Associated with a Poor Prognosis in Patients with Colorectal Cancer. Ann Surg Oncol. 2015;22: 1490–1498. doi:10.1245/s10434-015-4652-7

12. Sander EE, Grummt I. Oligomerization of the transcription termination factor TTF-I: Implications for the structural organization of ribosomal transcription units. Nucleic Acids Res. 1997;25: 1142–1147. doi:10.1093/nar/25.6.1142

13. Németh A, Guibert S, Tiwari VK, Ohlsson R, Längst G. Epigenetic regulation of TTF-I-mediated promoter-terminator interactions of rRNA genes. EMBO J. 2008;27: 1255–1265. doi:10.1038/emboj.2008.57

14. Boutin J, Lessard F, Tremblay MG, Moss T. The short N-terminal repeats of transcription termination factor 1 contain semi-redundant nucleolar localization signals and P19-ARF tumor suppressor binding sites. Yale J Biol Med. 2019;92: 385–396. Available: /pmc/articles/PMC6747939/

15. Jaiswal R, Choudhury M, Zaman S, Singh S, Santosh V, Bastia D, et al. Functional architecture of the Reb1-Ter complex of Schizosaccharomyces pombe. Proc Natl

Acad Sci U S A. 2016;113: E2267–E2276. doi:10.1073/pnas.1525465113

16. Park SH, Yu KL, Jung YM, Lee SD, Kim MJ, You JC. Investigation of functional roles of transcription termination factor-1 (TTF-I) in HIV-1 replication. BMB Rep. 2018;51: 338–343. doi:10.5483/BMBRep.2018.51.7.032

17. Singh SK, Sabatinos S, Forsburg S, Bastia D. Regulation of Replication Termination by Reb1 Protein-Mediated Action at a Distance. Cell. 2010;142: 868–878. doi:10.1016/j.cell.2010.08.013

18. Khor BY, Tye GJ, Lim TS, Choong YS. General overview on structure prediction of twilight-zone proteins. Theor Biol Med Model. 2015;12. doi:10.1186/s12976-015-0014-1

19. Chung SY, Subbiah S. A structural explanation for the twilight zone of protein sequence homology. Structure. 1996;4: 1123–1127. doi:10.1016/S0969-2126(96)00119-0

20. Roy A, Kucukural A, Zhang Y. I-TASSER: A unified platform for automated protein structure and function prediction. Nat Protoc. 2010;5: 725–738. doi:10.1038/nprot.2010.5

21. Yang J, Yan R, Roy A, Xu D, Poisson J, Zhang Y. The I-TASSER suite: Protein structure and function prediction. Nature Methods. Nat Methods; 2014. pp. 7–8. doi:10.1038/nmeth.3213

22. Kryshtafovych A, Schwede T, Topf M, Fidelis K, Moult J. Critical assessment of methods of protein structure prediction (CASP)—Round XIII. Proteins: Structure,

Function and Bioinformatics. Proteins; 2019. pp. 1011–1020. doi:10.1002/prot.25823

23. Rost B. Twilight zone of protein sequence alignments. Protein Eng. 1999;12: 85–94. doi:10.1093/protein/12.2.85

24. Krieger E, Joo K, Lee J, Lee J, Raman S, Thompson J, et al. Improving physical realism, stereochemistry, and side-chain accuracy in homology modeling: Four approaches that performed well in CASP8. Proteins: Structure, Function and Bioinformatics. Proteins; 2009. pp. 114–122. doi:10.1002/prot.22570

25. M W, MJ S. ProSA-web: interactive web service for the recognition of errors in three-dimensional structures of proteins. Nucleic Acids Res. 2007;35. doi:10.1093/NAR/GKM290

26. Zhang B, Ye W, Ye Y, Zhou H, Saeed AFUH, Chen J, et al. Structural insights into Cas13b-guided CRISPR RNA maturation and recognition. Cell Research. Cell Res; 2018. pp. 1198–1201. doi:10.1038/s41422-018-0109-4

27. Jumper J, Evans R, Pritzel A, Green T, Figurnov M, Ronneberger O, et al. Highly accurate protein structure prediction with AlphaFold. Nature. 2021;596: 583–589. doi:10.1038/s41586-021-03819-2

28. Gasteiger E, Hoogland C, Gattiker A, Duvaud S, Wilkins MR, Appel RD, et al. Protein Identification and Analysis Tools on the ExPASy Server. The Proteomics Protocols Handbook. Humana Press; 2005. pp. 571–607. doi:10.1385/1-59259-890-0:571

29. Jones DT, Cozzetto D. DISOPRED3: Precise disordered region predictions with annotated protein-binding activity. Bioinformatics. 2015;31: 857–863. doi:10.1093/bioinformatics/btu744

30. Ward JJ, McGuffin LJ, Bryson K, Buxton BF, Jones DT. The DISOPRED server for the prediction of protein disorder. Bioinformatics. 2004;20: 2138–2139. doi:10.1093/bioinformatics/bth195

31. Wiederstein M, Sippl MJ. ProSA-web: Interactive web service for the recognition of errors in three-dimensional structures of proteins. Nucleic Acids Res. 2007;35: W407-10. doi:10.1093/nar/gkm290

32. Laskowski RA, MacArthur MW, Moss DS, Thornton JM. PROCHECK: a program to check the stereochemical quality of protein structures. J Appl Crystallogr. 1993;26: 283–291. doi:10.1107/s0021889892009944

33. Zhang Y, Skolnick J. TM-align: A protein structure alignment algorithm based on the TM-score. Nucleic Acids Res. 2005;33: 2302–2309. doi:10.1093/nar/gki524

34. Zhang Y, Skolnick J. Scoring function for automated assessment of protein structure template quality. Proteins Struct Funct Genet. 2004;57: 702–710. doi:10.1002/prot.20264

35. Yang J, Roy A, Zhang Y. Protein-ligand binding site recognition using complementary binding-specific substructure comparison and sequence profile alignment. Bioinformatics. 2013;29: 2588–2595. doi:10.1093/bioinformatics/btt447

36. Zhang C, Freddolino PL, Zhang Y. COFACTOR: Improved protein function

prediction by combining structure, sequence and protein-protein interaction information. Nucleic Acids Res. 2017;45: W291–W299. doi:10.1093/nar/gkx366

37. Lu S, Wang J, Chitsaz F, Derbyshire MK, Geer RC, Gonzales NR, et al. CDD/SPARCLE: The conserved domain database in 2020. Nucleic Acids Res. 2020;48: D265–D268. doi:10.1093/nar/gkz991

38. Humphrey W, Dalke A, Schulten K. VMD: Visual molecular dynamics. J Mol Graph. 1996;14: 33–38. doi:10.1016/0263-7855(96)00018-5

39. Knapp B, Lederer N, Omasits U, Schreiner W. VmdICE: A plug-in for rapid evaluation of molecular dynamics simulations using VMD. J Comput Chem. 2010;31: 2868–2873. doi:10.1002/jcc.21581

40. Pettersen EF, Goddard TD, Huang CC, Couch GS, Greenblatt DM, Meng EC, et al. UCSF Chimera - A visualization system for exploratory research and analysis. J Comput Chem. 2004;25: 1605–1612. doi:10.1002/jcc.20084

41. Shannon P, Markiel A, Ozier O, Baliga NS, Wang JT, Ramage D, et al. Cytoscape: A software Environment for integrated models of biomolecular interaction networks. Genome Res. 2003;13: 2498–2504. doi:10.1101/gr.1239303

42. Doncheva NT, Klein K, Domingues FS, Albrecht M. Analyzing and visualizing residue networks of protein structures. Trends in Biochemical Sciences. Trends Biochem Sci; 2011. pp. 179–182. doi:10.1016/j.tibs.2011.01.002

Supporting information

S 1 Fig. Sequence-based representation of the disordered and protein binding regions of TTF1, as predicted using PsiPred.

S 2 Fig. Results of CD search indicating the presence of a SANT/Myb-like DNA-binding domain in TTF1.

S 1 Table. Occupancy of the hydrogen bonds formed by the central residues throughout the trajectory and in the last 50 ns.

Donor	Acceptor	Occupancy (200 ns)	Occupancy (last 50 ns)
K68*-Main	L67-Side	75.34%	85.41%
A175-Main	A176*-Main	76.84%	78.12%
R71*-Main	K68*-Main	77.29%	83.02%
S197-Side	E195*-Side	77.46%	99.50%
E27*-Main	I24-Main	77.51%	81.02%
D471*-Main	A469-Main	77.66%	97.60%
T896*-Main	N893*-Main	78.04%	97.60%
E882*-Main	E880-Side	78.41%	94.21%
D185-Side	N228*-Side	78.66%	82.72%
S227-Side	R229*-Side	79.01%	119.18%
K17*-Main	D16-Side	79.29%	91.01%
R182*-Side	N228*-Side	79.36%	80.92%
E431*-Main	A427-Main	79.41%	91.31%
E209-Main	E206*-Main	79.41%	93.61%
P437-Side	K434*-Main	79.76%	88.81%
W198*-Side	G202*-Main	79.94%	81.72%
I474-Main	D471*-Main	79.99%	90.11%
S197-Main	W198*-Main	80.58%	83.12%
A183-Main	R182*-Side	81.46%	75.82%
F657*-Main	K656-Side	82.58%	87.91%
E431*-Side	A427-Main	82.83%	117.98%
K18-Main	K17*-Side	83.03%	99.00%
P203-Side	W198*-Main	83.56%	125.27%
E35*-Main	H34*-Side	84.43%	82.82%
K31*-Side	E27*-Side	84.46%	125.47%
F657*-Main	V653-Main	84.53%	82.52%
R164*-Main	V163-Side	85.01%	94.91%
K31*-Main	H32-Main	85.61%	86.21%
E430-Main	E431*-Main	85.63%	90.91%
A176*-Main	S177-Main	86.01%	82.12%
S23*-Main	K19-Main	86.01%	100.00%
Q30*-Side	E27*-Main	86.23%	87.21%
S895*-Main	N893*-Side	86.26%	95.40%

K656-Main	F657*-Main	86.38%	86.81%
D471*-Main	S472-Main	86.66%	92.11%
V433-Main	K434*-Main	87.06%	82.32%
F657*-Side	V653-Main	87.33%	95.70%
K434*-Main	S435*-Main	87.43%	94.61%
S661-Side	F657*-Main	87.91%	78.82%
S33-Main	Q30*-Main	88.28%	90.11%
E27*-Main	R28-Main	88.51%	88.31%
A176*-Main	Q172*-Main	88.93%	95.00%
K31*-Side	E27*-Main	89.63%	85.31%
R438-Main	S435*-Main	89.68%	94.11%
D471*-Main	E467-Main	89.81%	90.51%
I660*-Main	F657*-Main	89.93%	93.61%
Q30*-Main	E27*-Main	90.08%	92.71%
P188-Side	N228*-Main	90.83%	115.78%
E431*-Main	G432-Main	91.03%	97.20%
S435*-Main	E431*-Main	91.05%	94.61%
R664*-Main	I660*-Main	91.45%	126.17%
E882*-Main	S881-Side	91.93%	94.71%
E35*-Main	I36-Main	92.25%	88.01%
Q181-Side	R182*-Main	92.65%	87.61%
T896*-Main	S895*-Side	92.85%	81.02%
K68*-Main	S65-Main	93.45%	84.82%
S435*-Main	K434*-Side	93.58%	96.20%
R229*-Main	N228*-Side	93.73%	97.80%
S661-Main	F657*-Main	93.83%	89.11%
I660*-Main	S661-Main	93.85%	98.60%
Q439-Main	S435*-Main	93.88%	92.51%
G901-Main	G899*-Main	94.28%	99.50%
E27*-Main	S23*-Main	94.65%	94.31%
A176*-Main	A175-Side	94.73%	97.70%
R71*-Main	S70-Side	95.15%	114.89%
S472-Main	D471*-Side	95.33%	93.91%
Q30*-Main	K31*-Main	95.33%	96.20%
I36-Main	E35*-Side	95.38%	92.11%
L62-Side	H34*-Main	95.68%	112.79%
E35*-Main	H32-Main	96.10%	91.71%
R436-Main	K434*-Main	96.93%	93.11%
S190-Main	E191*-Main	97.15%	97.20%
E470-Main	D471*-Main	97.18%	95.40%
E27*-Main	K26-Side	97.50%	96.80%
K26-Main	S23*-Main	97.68%	98.20%
H34*-Main	E35*-Main	97.73%	95.90%
I36-Main	H34*-Main	98.10%	123.08%
G432-Main	E431*-Side	98.18%	98.50%
K166-Main	E165*-Side	98.18%	99.30%
S435*-Main	R436-Main	98.25%	96.60%
D471*-Main	E470-Side	98.43%	97.00%
R173-Main	Q172*-Side	98.45%	104.40%
L67-Main	K68*-Main	98.55%	96.60%
S200-Main	E196*-Main	98.70%	96.50%
N228*-Main	T186*-Main	99.08%	99.90%
L199-Main	E195*-Main	99.18%	99.40%
T896*-Main	L897-Main	99.30%	96.60%
W198*-Main	E195*-Main	99.30%	99.50%
E195*-Main	Q194-Side	99.50%	99.40%
V201-Main	W198*-Main	99.55%	99.10%

W903-Main	R902*-Side	99.75%	100.30%
W198*-Main	L199-Main	99.80%	100.00%
K31*-Main	E27*-Main	99.85%	99.60%
T186*-Main	D185-Side	99.90%	99.90%
E195*-Main	K700-Main	99.98%	99.70%
D185-Main	T186*-Main	100.00%	100.00%
E165*-Main	K166-Main	100.02%	100.00%
T186*-Main	L187-Main	100.02%	100.10%
E195*-Main	E196*-Main	100.05%	100.10%
E230-Main	R229*-Side	100.07%	96.80%
Q194-Main	E195*-Main	100.07%	100.00%
H160-Main	S161*-Main	100.07%	100.10%
C892-Main	N893*-Main	100.22%	100.20%
R164*-Main	E165*-Main	100.27%	100.20%
R71*-Main	I72-Main	100.55%	101.20%
K26-Main	E27*-Main	100.57%	100.40%
S161*-Main	K162-Main	101.10%	100.10%
K31*-Main	Q30*-Side	101.15%	101.80%
C22-Main	S23*-Main	101.20%	105.19%
R229*-Main	E230-Main	101.22%	101.90%
E95-Main	L94-Side	101.35%	104.10%
D39-Main	R38*-Side	101.55%	102.80%
Q30*-Side	K31*-Main	101.65%	102.90%
F37-Main	R38*-Main	101.97%	114.59%
S227-Side	N228*-Main	102.00%	97.30%
N228*-Main	R229*-Main	102.32%	100.20%
S23*-Main	C22-Side	102.35%	94.41%
R436-Main	S435*-Side	102.40%	94.01%
V163-Side	R164*-Main	102.45%	96.60%
V201-Main	G202*-Main	102.62%	103.70%
K17*-Main	K18-Main	102.80%	96.40%
E430-Side	E431*-Main	102.85%	93.61%
R182*-Side	A176*-Main	102.90%	130.57%
K166-Main	E165*-Main	103.42%	102.20%
S192-Main	E191*-Side	103.70%	96.40%
N893*-Main	S894-Main	104.27%	104.10%
S33-Side	Q30*-Main	104.37%	95.00%
K68*-Main	K69-Main	104.37%	98.50%
F657*-Main	S658-Main	104.40%	100.70%
L67-Side	K68*-Main	104.57%	144.26%
S70-Main	R71*-Main	104.70%	95.10%
E191*-Main	S190-Side	105.00%	102.60%
G899*-Main	L897-Main	105.77%	158.34%
H32-Main	K31*-Side	105.95%	100.10%
H171-Main	Q172*-Main	106.65%	101.40%
L897-Main	S895*-Main	106.80%	133.17%
S895*-Side	E165*-Side	106.85%	204.70%
Q663-Main	R664*-Main	107.02%	117.68%
S881-Side	E882*-Main	107.50%	138.56%
E35*-Main	S33-Main	107.55%	100.40%
E431*-Main	E430-Side	107.60%	113.99%
R902*-Main	W903-Main	107.62%	104.10%
K225-Main	S226*-Main	107.67%	107.29%
S161*-Main	H160-Side	109.75%	95.40%
R28-Main	E27*-Side	110.17%	107.49%
S881-Main	E882*-Main	111.24%	105.79%
E882*-Main	G883-Main	111.49%	115.68%

K434*-Main	V433-Side	111.57%	127.37%
K434*-Side	Q663-Main	111.84%	118.18%
S227-Main	N228*-Main	113.14%	115.48%
Q30*-Main	P29-Side	113.47%	113.29%
S435*-Main	V433-Main	114.04%	104.90%
S226*-Main	K224-Main	114.97%	136.76%
K174-Main	Q172*-Main	115.02%	127.67%
K879-Side	R902*-Side	115.34%	217.68%
S895*-Side	T896*-Main	115.49%	80.92%
S661-Main	I660*-Side	115.52%	124.58%
R902*-Main	Q900-Main	116.44%	129.77%
I660*-Main	Q659-Side	116.72%	140.86%
E165*-Main	R164*-Side	117.87%	159.94%
S40-Main	R38*-Main	117.89%	130.77%
K434*-Main	G432-Main	118.02%	156.04%
V433-Main	E431*-Main	118.04%	109.99%
R38*-Side	E35*-Main	118.32%	105.09%
N893*-Side	R164*-Side	118.77%	215.38%
F37-Main	E35*-Main	118.79%	126.77%
W198*-Side	L199-Main	119.27%	118.88%
A176*-Side	Q172*-Main	119.49%	89.71%
F657*-Side	A454-Main	119.77%	171.13%
S435*-Side	R436-Main	120.59%	144.56%
R902*-Side	K879-Side	120.66%	247.15%
V433-Side	K434*-Main	120.76%	134.97%
R184-Main	R182*-Main	120.99%	114.99%
H34*-Main	S33-Side	122.36%	111.69%
E431*-Main	M429-Main	122.46%	117.48%
S70-Side	R71*-Main	122.59%	123.88%
T896*-Side	N893*-Main	123.06%	208.99%
K68*-Main	P66-Main	126.81%	99.40%
P29-Side	Q30*-Main	127.76%	125.87%
I660*-Side	S661-Main	127.76%	135.36%
R164*-Side	N893*-Side	128.19%	248.15%
I660*-Main	S658-Main	128.79%	173.53%
Q172*-Side	K803-Main	129.04%	122.78%
R38*-Main	I36-Main	129.06%	104.90%
K68*-Side	K69-Main	129.29%	105.89%
S33-Main	K31*-Main	131.36%	139.16%
S662-Main	I660*-Main	131.58%	86.01%
G202*-Main	W198*-Side	134.06%	118.28%
E206*-Main	G204-Main	134.06%	186.01%
N893*-Main	C892-Side	134.31%	126.77%
G205-Main	E206*-Main	134.93%	118.18%
E35*-Side	I36-Main	135.38%	125.47%
E191*-Side	S192-Main	135.86%	145.65%
K17*-Side	K18-Main	136.01%	134.17%
V163-Main	R164*-Main	136.38%	148.45%
R38*-Side	D39-Main	136.88%	107.79%
E196*-Side	S197-Main	137.48%	136.06%
H160-Side	S161*-Main	137.56%	185.51%
R182*-Side	A183-Main	137.63%	136.76%
C22-Side	S23*-Main	137.98%	153.55%
S197-Main	E196*-Side	138.01%	107.19%
R71*-Side	I72-Main	138.53%	132.07%
R664*-Main	N665-Main	138.96%	156.54%
S197-Side	W198*-Main	139.06%	130.97%

G202*-Main	W198*-Main	139.33%	141.26%
A176*-Side	S177-Main	139.86%	141.46%
W198*-Side	S699-Side	141.23%	190.21%
E431*-Side	G432-Main	141.73%	172.33%
S895*-Side	N893*-Side	141.73%	173.23%
S894-Side	S895*-Main	143.00%	136.36%
D16-Side	K17*-Main	143.30%	147.75%
K656-Side	F657*-Main	143.50%	157.84%
E473-Main	D471*-Main	143.68%	156.84%
S895*-Main	S894-Side	145.23%	128.37%
F657*-Main	L655-Main	145.63%	145.45%
R229*-Side	S227-Side	145.80%	215.18%
S161*-Side	K162-Main	146.63%	154.05%
Q663-Side	R664*-Main	146.88%	101.10%
I24-Main	S23*-Side	146.90%	160.14%
S435*-Side	E431*-Main	146.98%	139.66%
S23*-Side	I24-Main	148.58%	131.57%
T896*-Side	L897-Main	148.63%	178.42%
H32-Main	Q30*-Main	148.75%	144.16%
K434*-Side	S435*-Main	149.48%	165.43%
S894-Main	N893*-Side	150.75%	151.95%
W198*-Main	S197-Side	151.25%	157.04%
L897-Main	T896*-Side	152.00%	182.52%
Q194-Side	E195*-Main	152.55%	155.44%
R902*-Side	T896*-Main	152.85%	236.46%
A176*-Main	K174-Main	153.85%	155.94%
D471*-Side	S472-Main	154.42%	129.07%
E470-Side	D471*-Main	154.82%	117.38%
K167-Main	E165*-Main	154.90%	170.13%
Q659-Side	I660*-Main	156.85%	186.51%
G202*-Main	V201-Side	157.22%	152.05%
K31*-Side	H32-Main	157.72%	183.82%
G898-Main	G899*-Main	158.45%	136.66%
Q30*-Main	R28-Main	159.10%	163.44%
L199-Main	W198*-Side	159.12%	164.04%
S33-Side	H34*-Main	159.62%	156.54%
E206*-Side	I207-Main	159.67%	127.57%
V201-Side	G202*-Main	159.82%	169.03%
H193-Main	E191*-Main	160.04%	161.24%
T208-Main	E206*-Main	160.74%	192.31%
S70-Main	K68*-Main	161.44%	179.72%
H34*-Main	H32-Main	163.47%	161.64%
Q30*-Side	R71*-Main	165.09%	194.81%
R164*-Side	V163-Main	166.04%	191.01%
W198*-Main	E196*-Main	167.82%	178.82%
K162-Main	S161*-Side	168.42%	177.02%
K17*-Main	S15-Main	168.49%	147.05%
C892-Side	N893*-Main	168.52%	151.65%
H34*-Side	E35*-Main	168.84%	165.63%
D185-Side	T186*-Main	169.34%	169.83%
Q659-Main	F657*-Main	171.14%	183.42%
S190-Side	E191*-Main	171.89%	188.21%
S226*-Main	S227-Main	171.91%	160.04%
K391-Side	E431*-Side	173.11%	525.57%
Q172*-Main	H171-Side	174.26%	173.13%
K26-Side	E27*-Main	174.71%	170.13%
W178-Main	A176*-Main	174.79%	172.33%

S200-Side	E196*-Main	175.24%	167.83%
T896*-Main	S894-Main	175.56%	184.32%
G901-Main	R902*-Main	175.79%	185.51%
E27*-Side	R28-Main	176.59%	143.36%
R664*-Side	E453-Side	177.26%	163.94%
R229*-Side	E230-Main	178.89%	193.61%
E195*-Side	E196*-Main	181.06%	179.82%
N228*-Main	S227-Side	181.73%	188.41%
R164*-Side	E882*-Side	182.91%	338.56%
K434*-Side	E430-Main	183.93%	255.14%
S895*-Main	N893*-Main	184.93%	197.50%
N228*-Side	R229*-Main	185.01%	193.71%
L187-Main	T186*-Side	185.56%	190.91%
R902*-Side	W903-Main	186.46%	191.41%
Q172*-Side	R173-Main	186.56%	181.12%
R164*-Side	E165*-Main	187.01%	173.33%
A175-Side	A176*-Main	188.11%	193.61%
H25-Main	S23*-Main	189.38%	194.61%
W198*-Side	Q194-Side	190.18%	201.00%
G202*-Main	P203-Main	190.80%	196.10%
K17*-Side	E206*-Side	192.30%	445.15%
S197-Main	E195*-Main	193.05%	194.41%
G899*-Main	Q900-Main	194.33%	200.00%
E165*-Side	K166-Main	194.58%	198.40%
R182*-Main	S180-Main	194.80%	195.40%
N228*-Side	T186*-Main	197.88%	215.28%
S200-Main	W198*-Main	199.08%	198.20%
G202*-Main	P203-Side	199.68%	200.00%
P203-Main	G202*-Main	200.00%	200.00%
S226*-Main	K225-Main	200.12%	200.20%
R902*-Side	G901-Main	204.92%	249.75%
S649-Side	D471*-Side	208.30%	151.15%
K166-Side	E165*-Main	214.44%	215.08%
S699-Side	W198*-Side	215.84%	262.04%
R664*-Main	Q663-Main	217.54%	200.20%
K434*-Side	E431*-Side	222.09%	399.30%
K17*-Side	P13-Main	224.49%	154.05%
S226*-Side	K225-Main	227.46%	213.69%
K69-Side	E35*-Side	229.14%	129.47%
E196*-Main	E195*-Side	237.91%	280.82%
K17*-Side	P203-Main	239.81%	142.26%
N228*-Side	D185-Main	240.05%	254.15%
R664*-Side	Q663-Main	248.33%	260.14%
N615-Side	D471*-Side	252.77%	228.37%
K17*-Side	G204-Main	275.61%	254.55%
S227-Side	E191*-Side	276.89%	290.61%
K17*-Side	V201-Main	277.41%	122.28%
S227-Side	S226*-Main	278.39%	270.13%
R71*-Side	E9-Side	284.26%	79.12%
K434*-Side	E430-Side	288.83%	660.24%
K17*-Side	G202*-Main	295.48%	306.79%
T186*-Main	D185-Main	300.47%	300.50%
E195*-Main	Q194-Main	301.10%	301.20%
E165*-Main	R164*-Main	301.17%	300.40%
E196*-Main	E195*-Main	301.75%	300.40%
N893*-Main	C892-Main	304.20%	309.79%
L187-Main	T186*-Main	304.65%	302.40%

R229*-Main	N228*-Main	305.92%	302.10%
S161*-Main	H160-Main	306.82%	306.69%
W903-Main	R902*-Main	308.55%	304.20%
K162-Main	S161*-Main	312.37%	312.69%
Q900-Main	G899*-Main	312.69%	300.00%
N228*-Main	S227-Main	313.14%	315.48%
R164*-Side	E880-Side	313.72%	552.85%
Q172*-Main	H171-Main	336.23%	334.97%
I72-Main	R71*-Main	338.01%	341.26%
E206*-Main	G205-Main	340.43%	400.00%
S894-Main	N893*-Main	349.65%	346.95%
T186*-Side	L187-Main	359.20%	397.00%
R164*-Main	V163-Main	366.74%	361.24%
R902*-Side	E869-Side	380.26%	562.74%
R902*-Main	G901-Main	384.53%	400.00%
R229*-Side	E191*-Side	388.03%	500.00%
R182*-Side	E232-Main	389.63%	413.49%
N665-Main	R664*-Main	392.23%	400.00%
G432-Main	E431*-Main	399.93%	399.90%
R38*-Main	F37-Main	399.95%	400.00%
L897-Main	T896*-Main	400.00%	400.00%
T896*-Main	S895*-Main	400.00%	400.00%
S895*-Main	S894-Main	400.00%	400.00%
E882*-Main	S881-Main	400.00%	400.00%
R173-Main	Q172*-Main	400.00%	400.00%
E27*-Main	K26-Main	400.00%	400.00%
Q30*-Main	P29-Main	400.00%	400.00%
R28-Main	E27*-Main	400.00%	400.00%
S23*-Main	C22-Main	400.00%	400.00%
I24-Main	S23*-Main	400.00%	400.00%
H34*-Main	S33-Main	400.00%	400.00%
E35*-Main	H34*-Main	400.00%	400.00%
K31*-Main	Q30*-Main	400.00%	400.00%
H32-Main	K31*-Main	400.00%	400.00%
I36-Main	E35*-Main	400.00%	400.00%
A176*-Main	A175-Main	400.00%	400.00%
S177-Main	A176*-Main	400.00%	400.00%
K69-Main	K68*-Main	400.00%	400.00%
R71*-Main	S70-Main	400.00%	400.00%
S227-Main	S226*-Main	400.00%	400.00%
I207-Main	E206*-Main	400.00%	400.00%
K17*-Main	D16-Main	400.00%	400.00%
K18-Main	K17*-Main	400.00%	400.00%
K68*-Main	L67-Main	400.00%	400.00%
D39-Main	R38*-Main	400.00%	400.00%
E230-Main	R229*-Main	400.00%	400.00%
R182*-Main	Q181-Main	400.00%	400.00%
A183-Main	R182*-Main	400.00%	400.00%
L199-Main	W198*-Main	400.00%	400.00%
S192-Main	E191*-Main	400.00%	400.00%
E191*-Main	S190-Main	400.00%	400.00%
W198*-Main	S197-Main	400.00%	400.00%
S197-Main	E196*-Main	400.00%	400.00%
E431*-Main	E430-Main	400.00%	400.00%
R436-Main	S435*-Main	400.00%	400.00%
S435*-Main	K434*-Main	400.00%	400.00%
K434*-Main	V433-Main	400.00%	400.00%

S658-Main	F657*-Main	400.00%	400.00%
I660*-Main	Q659-Main	400.00%	400.00%
F657*-Main	K656-Main	400.00%	400.00%
S661-Main	I660*-Main	400.00%	400.00%
D471*-Main	E470-Main	400.00%	400.00%
S472-Main	D471*-Main	400.00%	400.00%
G899*-Main	G898-Main	400.10%	401.00%
G202*-Main	V201-Main	400.82%	403.30%
R38*-Side	E35*-Side	406.17%	385.11%
R229*-Side	N228*-Main	421.29%	512.19%
R164*-Side	E165*-Side	457.75%	489.11%
G883-Main	E882*-Main	472.74%	561.44%
K20-Side	E27*-Side	530.31%	389.51%
P203-Side	G202*-Main	601.07%	602.20%
K765-Side	E206*-Side	655.37%	665.53%

The central residues are marked by *. Side and Main indicate whether the hydrogen bond was formed with an atom of the side chain or the main chain, respectively. Occupancies >100% indicate the formation of more than one inter-residue hydrogen bond.

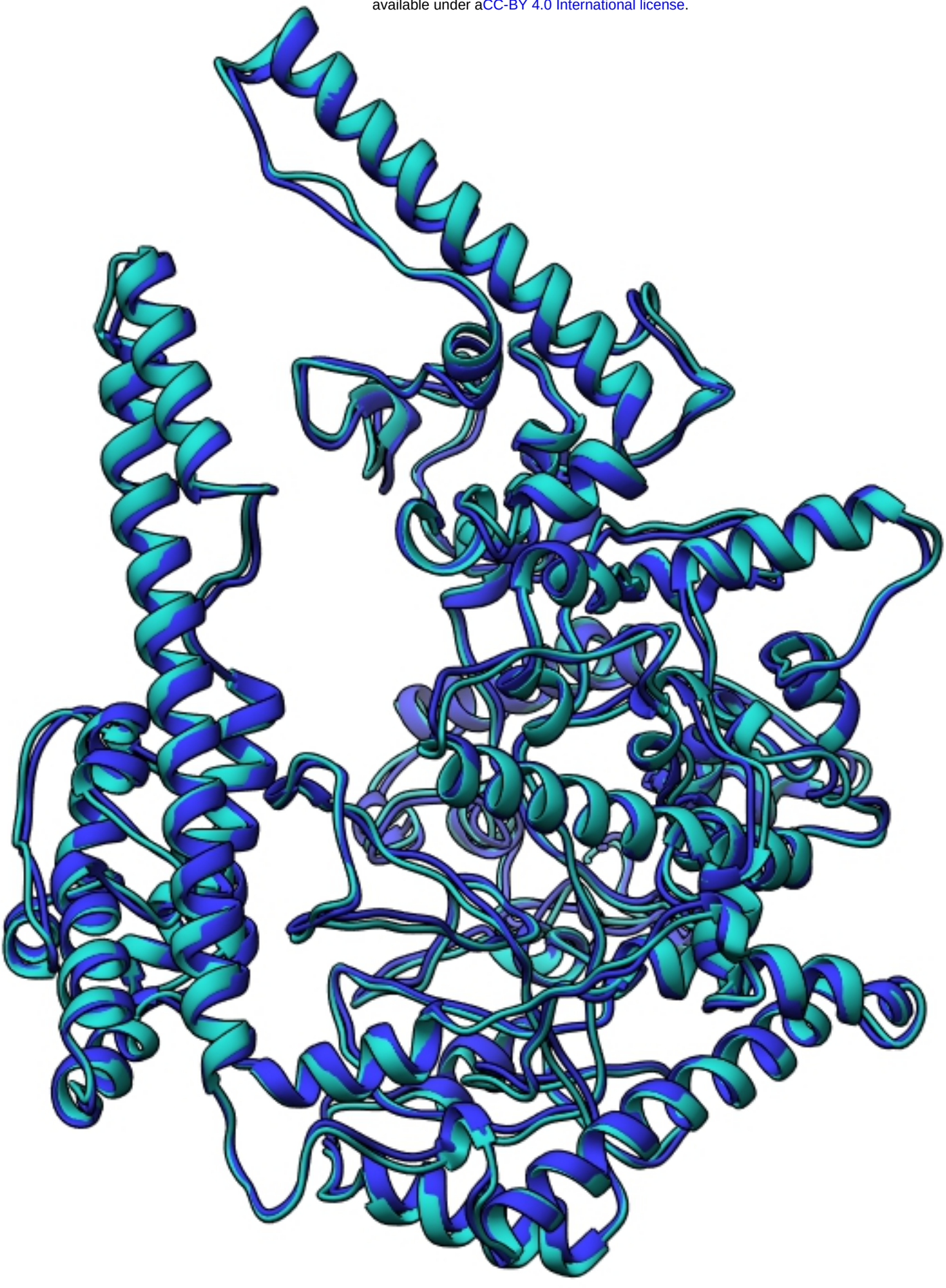

Fig 3

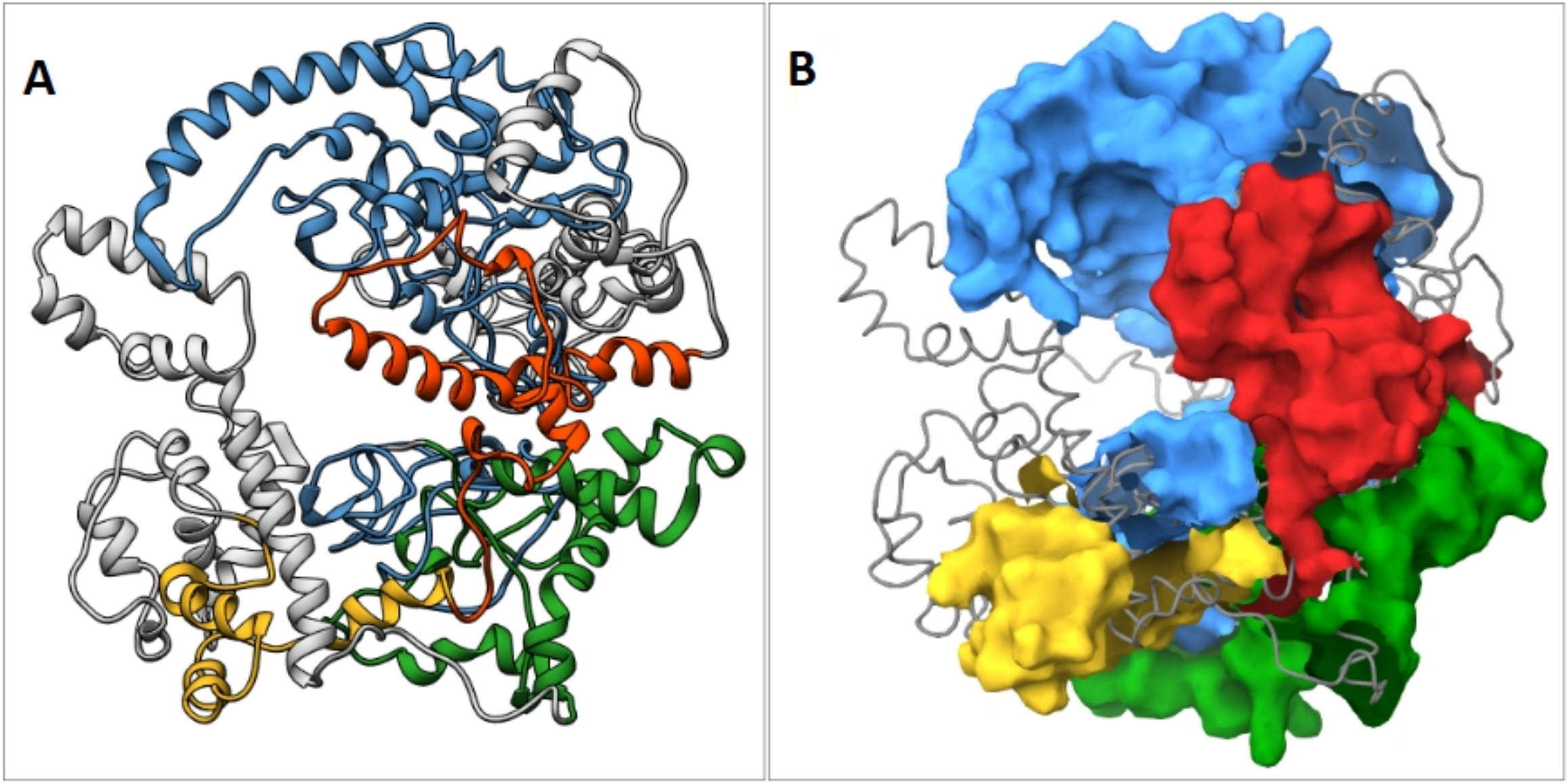

Fig 5

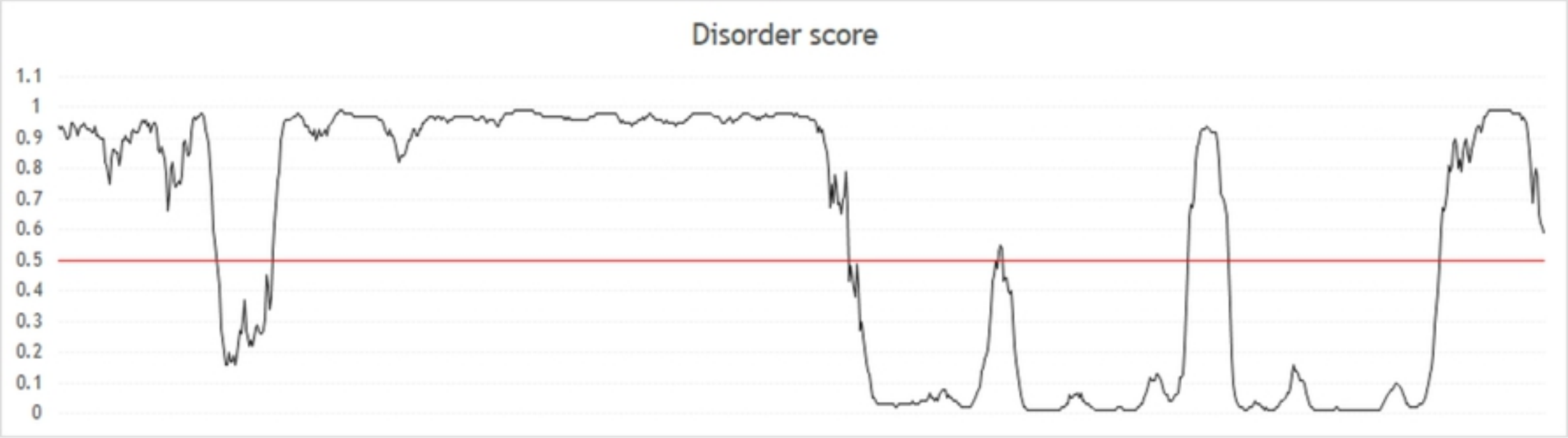

Fig 1

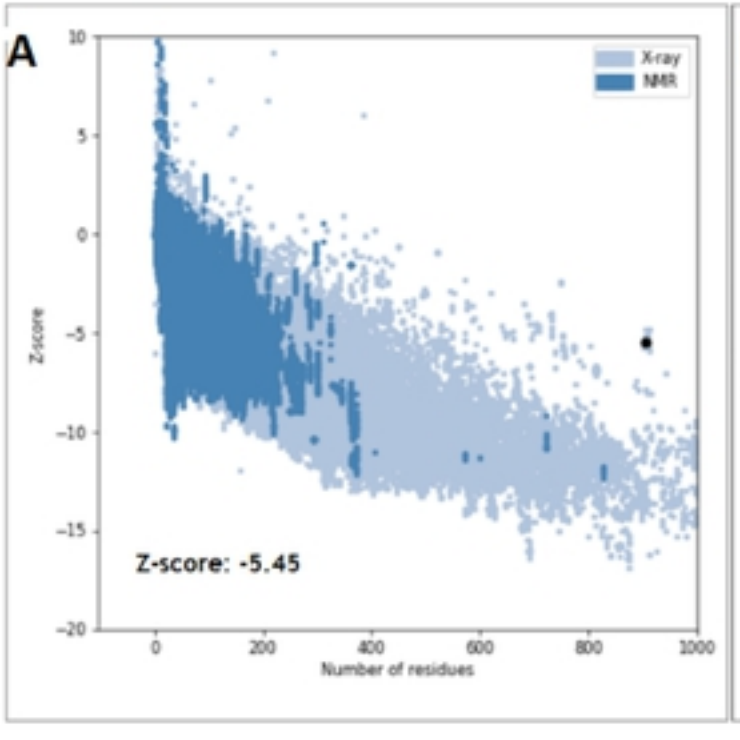

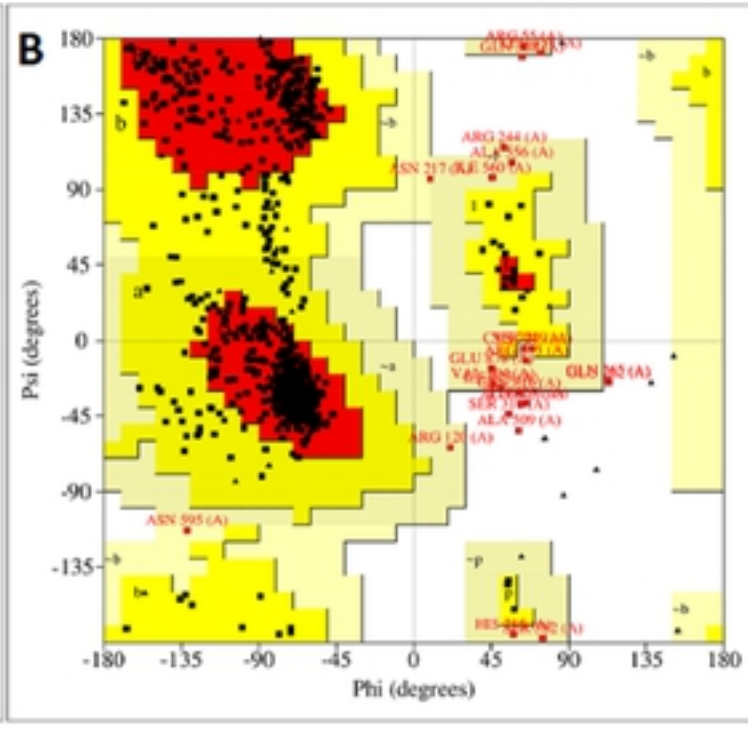

Residues in most favoured regions [A,B,L]	680	82.9%
Residues in additional allowed regions [a,b,l,p]	116	14.1%
Residues in generously allowed regions [~a,~b,~l,~p]	16	2.0%
Residues in disallowed regions	8	1.0%
Number of non-glycine and non-proline residues	820	100.0%
Number of end-residues (excl. Gly and Pro)	2	
Number of glycine residues (shown as triangles)	46	
Number of proline residues	37	
Total number of residues	905	

Fig 2

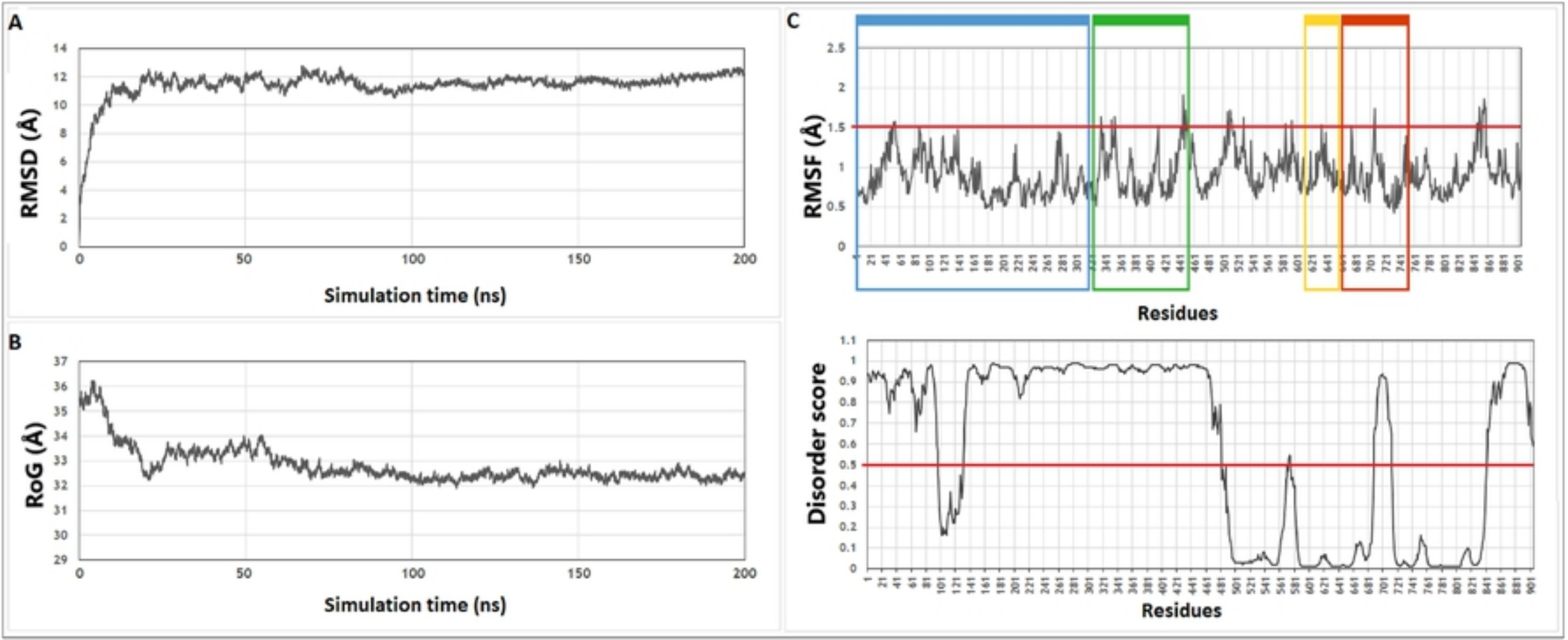
A
RMSD (Å)
Simulation time (ns)
B
RoG (Å)
Simulation time (ns)
C
RMSF (Å)
Residues
Disorder score
Residues

Fig 4

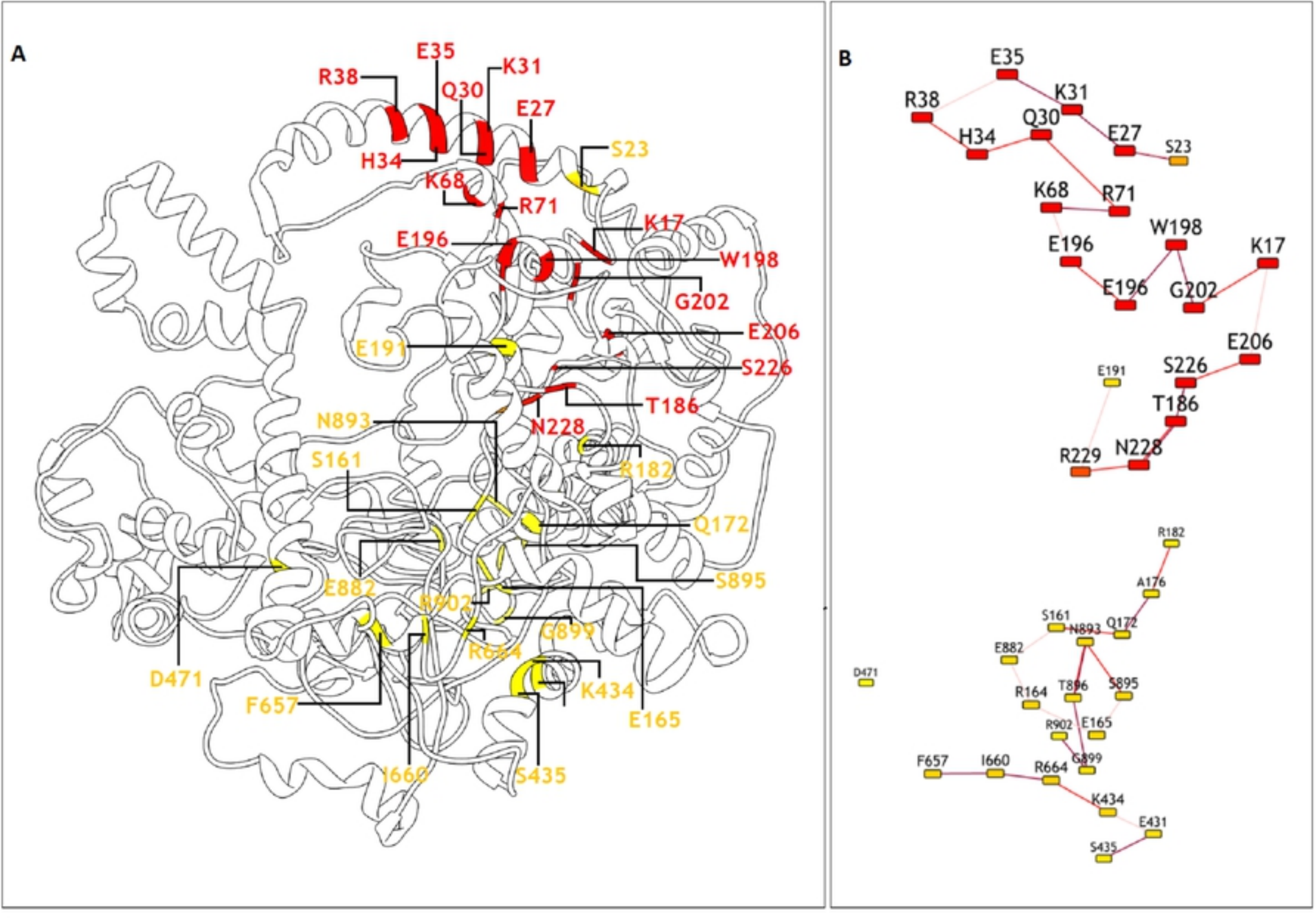
A
E35
R38
K31
Q30
E27
H34
S23
K68
R71
K17
E196
W198
G202
E206
E191
S226
T186
N893
N228
S161
R182
Q172
S895
E882
R902
G899
R664
D471
K434
F657
E165
I660
S435
B
E35
R38
K31
Q30
H34
E27
S23
K68
R71
W198
E196
K17
E196
G202
E206
E191
S226
T186
R229
N228
R182
A176
S161
N893
Q172
E882
D471
R164
T896
S895
R902
E165
F657
I660
R664
G899
K434
E431
S435

Fig 6

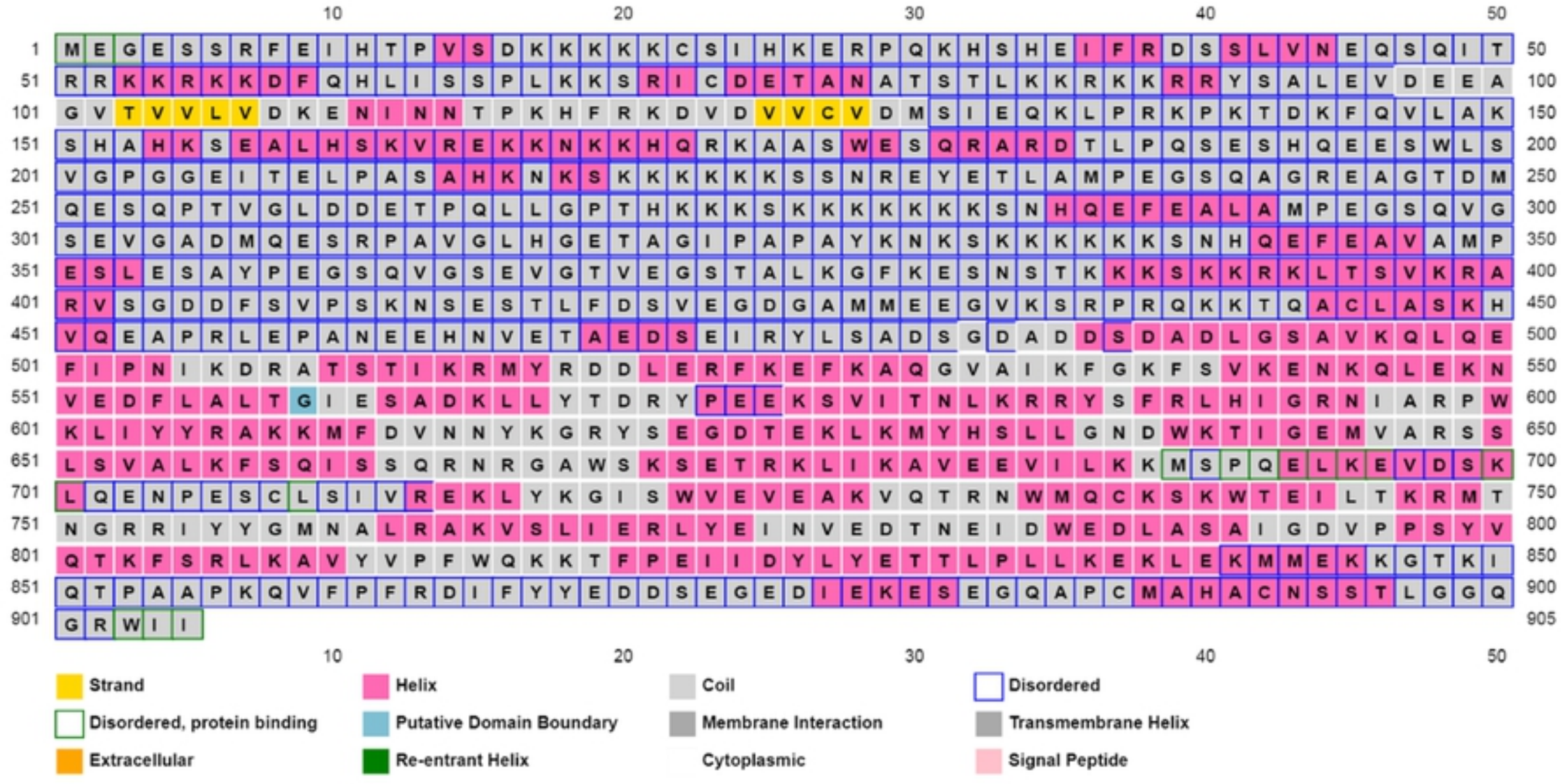
10
20
30
40
50
1 M E G E S S R F E I H T P V S D K K K K K C S I H K E R P Q K H S H E I F R D S S L V N E Q S Q I T 50
51 R R K K R K K D F Q H L I S S P L K K S R I C D E T A N A T S T L K K R K K R R Y S A L E V D E E A 100
101 G V T V V L V D K E N I N N T P K H F R K D V D V V C V D M S I E Q K L P R K P K T D K F Q V L A K 150
151 S H A H K S E A L H S K V R E K K N K K H Q R K A A S W E S Q R A R D T L P Q S E S H Q E E S W L S 200
201 V G P G G E I T E L P A S A H K N K S K K K K K K K S S N R E Y E T L A M P E G S Q A G R E A G T D M 250
251 Q E S Q P T V G L D D E T P Q L L G P T H K K K S K K K K K K K K S N H Q E F E A L A M P E G S Q V G 300
301 S E V G A D M Q E S R P A V G L H G E T A G I P A P A Y K N K S K K K K K K K S N H Q E F E A V A M P 350
351 E S L E S A Y P E G S Q V G S E V G T V E G S T A L K G F K E S N S T K K K S K K R K L T S V K R A 400
401 R V S G D D F S V P S K N S E S T L F D S V E G D G A M M E E G V K S R P R Q K K T Q A C L A S K H 450
451 V Q E A P R L E P A N E E H N V E T A E D S E I R Y L S A D S G D A D D S D A D L G S A V K Q L Q E 500
501 F I P N I K D R A T S T I K R M Y R D D L E R F K E F K A Q G V A I K F G K F S V K E N K Q L E K N 550
551 V E D F L A L T G I E S A D K L L Y T D R Y P E E K S V I T N L K R R Y S F R L H I G R N I A R P W 600
601 K L I Y Y R A K K M F D V N N Y K G R Y S E G D T E K L K M Y H S L L G N D W K T I G E M V A R S S 650
651 L S V A L K F S Q I S S Q R N R G A W S K S E T R K L I K A V E E V I L K K M S P Q E L K E V D S K 700
701 L Q E N P E S C L S I V R E K L Y K G I S W V E V E A K V Q T R N W M Q C K S K W T E I L T K R M T 750
751 N G R R I Y Y G M N A L R A K V S L I E R L Y E I N V E D T N E I D W E D L A S A I G D V P P S Y V 800
801 Q T K F S R L K A V Y V P F W Q K K T F P E I I D Y L Y E T T L P L L K E K L E K M M E K K G T K I 850
851 Q T P A A P K Q V F P F R D I F Y Y E D D S E G E D I E K E S E G Q A P C M A H A C N S S T L G G Q 900
901 G R W I I 905
10
20
30
40
50
Strand
Helix
Coil
Disordered
Disordered, protein binding
Putative Domain Boundary
Membrane Interaction
Transmembrane Helix
Extracellular
Re-entrant Helix
Cytoplasmic
Signal Peptide

S 1 Fig

Protein Classification

SANT/Myb-like DNA-binding domain-containing protein (domain architecture ID 10621698)
SANT/Myb-like DNA-binding domain-containing protein binds DNA and may function as a transcription factor

Graphical summary

Zoom to residue level | show extra options »

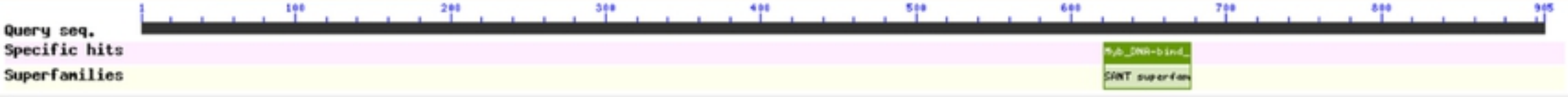

List of domain hits

Name	Accession	Description	Interval	E-value
[+] Myb_DNA-bind_6	pfam13921	Myb-like DNA-binding domain; This family contains the DNA binding domains from Myb proteins, ...	621-677	2.95e-08

S 2 Fig